Microstructure Characterization and Creep Behavior of Pb-Free Sn-Rich Solder Alloys: Part II. Creep Behavior of Bulk Solder and Solder/Copper Joints

R.S. SIDHU, X. DENG, and N. CHAWLA

Microstructure plays a critical role in the mechanical behavior of Sn-rich solder alloys. A unified mechanistic understanding of creep in Sn-rich solder alloys, at various microstructural length scales, is missing. Part I of this study focused on microstructure characterization of Sn-rich solder alloys. Part II focuses on the creep behavior of bulk solder alloys and small solder joints comparable in size and geometry to those in electronic packages. Pure Sn, Sn-0.7Cu, Sn-3.5Ag, and Sn-3.9Ag-0.7Cu were used in these studies. At the bulk level, creep appears to be controlled by subgrain formation, whose size is controlled by Ag_3Sn orCu_6Sn_5 particles. At the smaller joint level, where the microstructures are much finer, creep in Ag-containing alloys was controlled by local climb and detachment along Ag_3Sn particles. The threshold stress for creep is inversely proportional to the Ag_3Sn interparticle spacing. At the joint level, the creep of Sn and Sn-Cu alloys was controlled by viscous flow at grain boundaries at low stress, and transition to dislocation climb at higher stress.

DOI: 10.1007/s11661-007-9412-2
© The Minerals, Metals & Materials Society and ASM International 2007

I. INTRODUCTION

SOLDERS are an important part of electronic packages because they serve as mechanical and electrical interconnects.[1–5] During device operation, creep (long-term stress at temperatures greater than half the homologous melting point) and fatigue damage (thermomechanical cyclic stress) occur in solder joints due to the coefficient of thermal expansion (CTE) mismatch between the different materials in the electronic package.

As described in the companion article,[6] there is a significant driving force toward developing high-performance, environmentally-benign, Pb-free solder alloys. Among several potential Pb-free solders, Sn-rich solders (Sn-Ag, Sn-Cu, and Sn-Ag-Cu) have been broadly targeted as potential candidates for replacement of the Sn-Pb system.[1,4] These solders have emerged as promising alternatives because of their higher strength, superior resistance to creep and thermal fatigue, and adequate cost.[1–5] The mechanical properties of the solder are strongly influenced by microstructure, which is controlled by thermal history, *i.e.*, solidification rate and aging. Thus, an understanding of the relationship between microstructure (as controlled by cooling rate of the solder) and mechanical behavior of Sn-rich solders is extremely important.

Several studies have examined the creep behavior of Sn-rich solders in both bulk[7–20] and solder joint[21–28] form. A comparison of work in the literature shows that there is a profound difference in creep behavior between the bulk material (thickness ~2 to 6 mm) and solder joints, which are more comparable in size and geometry to actual solder balls found in electronic packages (diameter < 1 mm). The relationship between bulk and small solder joint creep behavior is not trivial, as the creep behavior depends on several important variables including microstructure, stress state, and testing geometry. Tables I and II provide a summary of creep stress exponents reported for bulk and small solder joint samples for a given temperature range. In an attempt to correlate the microstructure and creep behavior, the secondary Sn-dendrite size and intermetallic particle size were estimated from micrographs from the respective reports wherever possible.

An examination of the creep-rate stress exponents (n) for Sn-rich alloys is quite broad, spanning from 3 to 18.[7–29] Similarly, the activation energies (E_a) in Sn-rich solders have been reported in the range of 39 to 135 kJ/mol.[1,7–29] The large range in n and E_a may indicate that different creep mechanisms (*i.e.*, dislocation climb, grain boundary sliding, and viscous glide) are taking place. Kerr and Chawla[21] studied the creep behavior of single Sn-Ag/Cu solder joints. Their microstructure consisted of Sn-dendrites and a eutectic mixture of fine Ag_3Sn particles (< 85 nm) in a Sn matrix. Creep data showed a well-defined low-stress (n = 4 to 6) and high-stress (n = 14 to 20) regime. It was suggested that the high-stress regime was caused by Ag_3Sn particles acting as barriers to dislocation motion and analyzed

R.S. SIDHU, formerly Graduate Research Assistant, School of Materials, Fulton School of Engineering, Arizona State University, is with Assembly Technology Development, Intel Corp., Chandler, AZ, USA. X. DENG, formerly Postdoctoral Fellow, School of Materials, Fulton School of Engineering, Arizona State University, is with Kennametal Corp., Rogers, AK, USA. N. CHAWLA, Professor, is with the School of Materials, Fulton School of Engineering, Arizona State University, Tempe, AZ 85287-8706, USA. Contact e-mail: nchawla@asu.edu

Manuscript submitted January 12, 2006.
Article published online December 8, 2007

Table I. Summary of Creep-Stress Exponents for Bulk Samples in Tension

Reference	Material System	Creep Stress Exponent (n)	Temperature Range (°C)	Approximate Intermetallic Size (μm)	Approximate Secondary Sn-Dendrite Size (μm)
Ochoa *et al.*[7]	Sn-3.5Ag	7 to10	25 to 120	0.3 to 20	3 to 9
Wu and Huang[8]	Sn-0.7Cu	7 to 12	30 to 120	—	50
Mathew *et al.*[9]	Sn and Sn-3.5Ag	5 to 7	23 to100	—	15
Mavoori *et al.*[10]	Sn-3.5Ag	12	25 to 80	—	—
Wu *et al.*[11]	Sn-3.5Ag	11	105	0.5	20
McCabe and Fine[12]	Sn	6 to 8	23 to 101	—	—
Vianco *et al.*[13,14]	Sn-3.9Ag-0.6Cu	4 to 7	–25 to 160	—	40
Xiao and Armstrong[15]	Sn-3.9Ag-0.6Cu	4 to 11	45 to 150	—	10
Wade *et al.*[16]	Sn-0.5Cu, Sn-3.5Ag, and Sn-3.5Ag-0.5Cu	8 to 13	105 to 130	0.5	30
Joo *et al.*[17]	Sn-3.5Ag-(0 to 1.5)Cu	4 to 8	100	1	20 to 100
El-Bahay *et al.*[18]	Sn-3.5Ag	3 to 9	200 to 220	—	—
Kariya *et al.*[19]	Sn-3.0Ag-0.5Cu	9 to 13	25 to 75	—	10 to 20
Raeder *et al.*[20]	Sn-3.5Ag	6 to 8	20 to 158	—	—

Table II. Summary of Creep-Stress Exponents for Solder Joint Samples

Reference	Material System	Creep Exponent (n) Low Stress	Temperature Range (°C)	Creep Exponent (n) High Stress	Temperature Range (°C)	Approximate Intermetallic Size (μm)	Approximate Secondary Sn-Dendrite Size (μm)
Kerr and Chawla[21]	Sn-3.5Ag	4 to 6	25 to 130	14 to 20	25 to 130	0.06 to 0.09	4 to 6
Rhee *et al.*[22]	Sn-3.5Ag and Sn-4Ag-0.5Cu	6 to 12	25 to 150	—	—	—	15
Jadhav *et al.*[23]	Sn-3.5Ag	5	50	7 to 9	150		
Lau *et al.*[24]	Sn-3.5Ag	5	50	—	—	—	—
Song *et al.*[25]	Sn-3.5Ag, Sn-0.7Cu, and Sn-3Ag-0.5Cu	4 to 6	60 to 130	7 to 12	60 to 130	—	—
Shin and Yu[26]	Sn-3.5Ag and Sn-3.5Ag-0.75Cu	6	100	9 to 13	100	—	10
Darveaux *et al.*[27]	Sn-3.5Ag and Sn-4Ag-0.5Cu	—	—	11 to 18	27	—	—
Weise *et al.*[28]	Sn-3.5Ag and Sn-4Ag-0.5Cu	3		11 to 12		<0.2	—

by a threshold stress analysis. Dislocation climb was cited as the predominant mechanism controlling creep deformation in the low-stress regime. Climb-controlled deformation during creep has also been postulated as an operative mechanism by Wu and Huang[8] and Mathew *et al.*,[9] although these studies were conducted in bulk solder. In fact, in these bulk solder studies, a single creep-stress exponent was observed over the entire stress range. It is possible that this may be due to the bulk solders having a much coarser microstructure (secondary Sn dendrite size ~15 to 50 μm) compared to the solder joint (secondary Sn dendrite size ~4 to 6 μm). At temperatures close to the Sn-3.5Ag solder melting point (200 °C to 220 °C), it has been proposed that creep deformation was due to viscous glide ($n = {\sim}3, Q = {\sim}30$ kJ/mol).[18] It has also been postulated that the operative mechanism for creep deformation in Sn-rich alloys may be grain boundary sliding along Sn-Sn grain boundaries.[22,30] However, Ochoa *et al.*[7] used scanning electron microscopy and atomic force microscopy to show that the contribution of grain boundary sliding to the total creep strain in Sn-3.5Ag solder is very small (~ $<$ 8 pct total strain).

Several diffusion mechanisms have been reported for Sn-rich alloys.[7–28] For bulk Sn-rich solders, dislocation core diffusion (Q = ~50 to 70 kJ/mol)[7,9,12,15] or lattice diffusion (Q = ~100 to 120 kJ/mol)[8,10] have been reported as the operative diffusion mechanism over a wide temperature range (25 °C to 120 °C). Interestingly, in other reports diffusion mechanisms have been shown to be influence by temperature[13,14,21,28] with two separate processes involved during creep. At low temperatures ($<$ 75 °C) creep is controlled by dislocation core diffusion and at high temperatures ($>$ 75 °C) creep is controlled by lattice diffusion. It is clear that there are several discrepancies between studies of Sn-rich alloys containing Ag and Cu. Since very few of these studies provide an in-depth quantification of the microstructure, it is difficult to decipher the influence of specific microstructure feature on the creep behavior. Thus, upon reviewing the literature, we can conclude that a unified mechanistic understanding of creep in Sn-rich solder alloys is still required.

A comprehensive study is necessary to determine the relationship between microstructure (*i.e.*, intermetallic

particle size and spacing), creep stress exponents, and activation energies. Particular attention needs to be paid to dislocation-particle interactions to help rationalize the high-stress exponents ($n > 10$) observed in these systems. In this article, which is Part II of our study, we provide a comprehensive understanding of the creep behavior for Sn-rich solder alloys. Bulk solder creep behavior is compared to small solder sphere joint creep behavior, where the solder joints are analogous in size and geometry to those employed in electronic packages. We refer to the comprehensive microstructure characterization detailed in Part I[6] to draw conclusions regarding the relationship between creep behavior and microstructure. The underlying mechanisms for creep deformation in bulk Sn-rich solders and small solder joints will be determined by invoking a subgrain and threshold stress analysis to account for anomalously high-creep stress exponents. Theoretical deformation models will then be used to explain and predict the magnitude of the threshold stress in terms of dislocation-particle interactions. Finally, the postulated creep mechanisms were studied and verified by transmission electron microscopy (TEM) of crept samples.

II. EXPERIMENTAL PROCEDURE

Characterization of the creep behavior of bulk solder and small solder joints was conducted on four materials: pure Sn, Sn-0.7Cu, Sn-3.5Ag, and Sn-3.9Ag-0.7Cu. Detail on sample fabrication and reflow for both bulk and solder joints are provided in Part I of this study.[6]

Creep testing of the small solder joints was conducted on a micromechanical testing system (TYTRON*) at temperatures of 25 °C, 60 °C, 95 °C, and 130 °C. The system consists of an actuator that incorporates a thin-film air bearing for near friction-free operation.[31,32] A DC linear motor function enables application of displacement through the actuator assembly. The strain was measured using a high-resolution displacement gage, with a sensitivity of about 0.1 μm. The load was measured using a ± 250 N load cell with a resolution of ± 0.1 N. A convection air furnace was used to control the temperature during the creep tests, and samples were secured with water-cooled grips. The temperature variability in the solder, measured with a thermocouple close to the sample, was approximately ± 0.1 °C. To compensate for variability in solder joint geometry, the joint thickness and pad size were measured in each sample in order to accurately measure the applied stress and strain.

*TYTRON is a trademark of MTS Systems, Minneapolis, MN.

Bulk creep specimens were machined into dogbone specimens 10 cm in length, 0.4 cm in thickness, and with a gage length of 3.2 cm. The samples were machined from the bottom of reflowed blanks (Indium Corp, Ithaca, NY), where the microstructure was relatively homogenous. Creep tests were conducted at 25 °C, 95 °C, and 120 °C on a servohydraulic load frame. The creep experiments were conducted using a box furnace and water-cooled grips. The strain was measured with a clip-on extensometer with a gage length of 2.5 cm and a sensitivity of about 2 μm. The specimen temperature was monitored using a thermocouple located near the middle of the gaged section of the specimen, and was approximately ± 0.5 °C. Additional creep testing of the bulk solder microstructure was conducted on the TYTRON using smaller tensile specimens with a gage section width of 2.4 mm, thickness of 0.5 mm, and length of 20 mm. This was conducted to minimize the sample-to-sample variability that was observed in the larger bulk specimens due to processing (*i.e.*, internal porosity, flaws within gage section, *etc.*)

The activation energy during creep was determined using two separate methods:[33,34] (1) constant stress experiments, where the temperature of the sample at constant stress was incrementally increased and the strain rate measured; and (2) conventional constant stress, constant temperature experiments. The purpose of utilizing the first method was to ensure that the activation energy for creep was not structure-dependent and microstructure coarsening was not influencing the apparent diffusion mechanism. After creep TEM was conducted. Details of TEM sample preparation are provided in Part I.[6]

III. RESULTS AND DISCUSSION

The presentation of creep results is divided in terms of (a) bulk solder and (b) small-scale solder sphere joints. Within each section, the creep behavior is characterized in terms of creep stress exponents, activation energies for creep, and TEM of crept samples. Analytical and numerical models were used to explain the experimentally-observed trends. The authors have also previously studied the creep behavior of Sn-3.5Ag both in bulk form[7] and in solder joints.[32] These studies are included as a means of comparison. Section III-B discusses the unification of bulk and small-scale length creep behavior in terms of the relevant microstructural parameters and their length scales.

A. *Creep Behavior of Bulk Solder*

As shown in Part I[6] of this study, the size of Ag_3Sn particles for bulk, water-quenched, and solder joints was quite fine, on the order of 100 to 200 nm, while those in furnace-cooled samples were much coarser, on the order of 10 to 17 μm. It is interesting to note that there was no difference in Ag_3Sn particle size and aspect ratio between Sn-Ag and Sn-Ag-Cu alloys. The aspect ratio of Ag_3Sn in the finer microstructures was on the order of 1 to 2, indicating that the particles were somewhat spherical. On the other hand, furnace cooling provided sufficient time for diffusion and particle growth to take place, resulting in Ag_3Sn rodlike structures (*i.e.*, much higher aspect ratio). Slower cooling also resulted in an increase in interparticle spacing, which is directly related

to particle size. These differences in microstructure had a profound effect on the creep resistance.

The creep behavior of bulk Sn, Sn-0.7Cu, and Sn-3.9Ag-0.7Cu solder systems was studied at 25 °C, 95 °C, and 120 °C. The steady-state creep rate *vs* applied stress was used to obtain the creep stress exponent, n. The steady-state strain rate during creep can be related to the applied stress by the Mukherjee–Bird–Dorn equation:[35]

$$\dot{\varepsilon}_S = A\left(\frac{G\mathbf{b}}{\mathrm{R}T}\right)\left(\frac{\sigma}{G}\right)^n \exp\left(\frac{-Q_c}{\mathrm{R}T}\right) \qquad [1]$$

where $\dot{\varepsilon}_s$ is the minimum steady-state strain rate, Q_c denotes the activation energy for creep, σ is the applied stress, n is the creep stress exponent, G is the temperature-dependent shear modulus, **b** is the burger's vector, R is the gas constant, T is the temperature in Kelvin, and A is a constant. The creep rate *vs* applied stress data for the four alloys in bulk form are shown in Figure 1. Figure 1(a) through (d) show the data for samples cooled at 0.1 °C/s (furnace-cooled), while Figure 1(e) through (h) show creep data for samples at 24 °C/s (water-quenched). The Sn exhibited the highest creep rate followed by Sn-Cu, Sn-Ag, and Sn-Ag-Cu for samples at both cooling rates.

A summary of the creep-stress exponents is shown in Table III. For the bulk 0.1 °C/s cooled samples, the n exponent is ~7, while for 24 °C/s it ranges from 7 to 10. These values fall within the wide range of reported stress exponents for bulk Sn-rich solder alloys (n = 3 to 13).[7–20] Bulk pure Sn system exhibited an n exponent of 7, independent of cooling rate. This correlates well with other studies on bulk pure Sn, where stress exponents of 7 have also been reported.[9,12] The value of the stress exponent indicates dislocation climb as the predominant mechanism for creep. This is discussed in more detail later in this section.

It is interesting to note that in general the bulk Sn-rich alloys, while exhibiting better creep resistance than pure Sn, had stress exponents similar to that of pure Sn. This is more so the case in the slower cooled samples (1 °C/s), which had a coarser microstructure consisting of large Sn-dendrites and widely dispersed Cu_6Sn_5 or Ag_3Sn needles intermetallics. The Sn-Ag and Sn-Ag-Cu materials cooled at 24 °C/s, *i.e.*, materials with a finer microstructure behaved more like dispersion-strengthened alloys. In these alloys the creep resistance increased significantly due to the very fine scale of Ag_3Sn, which had a size of 200 to 250 nm and interparticle spacing of < 265 nm. Some evidence of this can also be seen in the slight increase in the stress exponent to 10 at ambient temperature.

Measurements of activation energy were taken for the bulk solder cooled at 0.1 °C/s, since the stress exponents were constant at all temperatures. The activation energies were between ~52 to 67 kJ/mol for all four solders in the temperature range of 25 °C to 120 °C (Table IV). These values compare well with recent studies on bulk Sn-rich alloys where the activation energy ranged from 55 to 77 kJ/mol.[9,15,17] Furthermore, they are consistent with the activation energy required for dislocation core diffusion in pure Sn, which is in the range of 50 to 70 kJ/mol.[9,36–38] Thus, for the temperature range in the present study, dislocation-core diffusion appears to be the dominant diffusion mechanism during creep in the bulk specimens. It is important to note that although the small quantities of alloying additions have a significant effect on creep resistance, they seem to have a minimal effect on the diffusion mechanism in bulk Sn-rich solders.[39]

An analysis of the creep-stress exponents and activation energy for creep showed that creep appears to be taking place by dislocation climb, with diffusion taking place through the cores of dislocations. Sherby and coworkers,[40–43] demonstrated that when well defined subgrain boundaries form during creep a marked change in the stress exponent occurs from n = ~5 to 8. The exact mechanism for subgrain formation is not fully understood, although it is generally agreed that subgrains are associated with slip bands.[44,45] Furthermore, second-phase particles, such as Ag_3Sn in Sn-Ag and Sn-Ag-Cu, or Cu_6Sn_5 and grain boundaries in Sn-Cu and pure Sn, can act as pinning sites that define the area of subgrains.[45] The influence of subgrain size during creep can be described as follows:[40]

$$\dot{\varepsilon} = K\left(\frac{\lambda^3}{\mathbf{b}}\right)\frac{D_{\mathrm{eff}}}{\mathbf{b}^2}\left(\frac{\sigma}{G}\right)^8 \qquad [2]$$

where **b** is the burgers's vector, G is the shear modulus, λ is the subgrain or barrier distance (in our case, the interparticle spacing), and D_{eff} is the effective diffusion coefficient. The creep exponent ($\dot{\varepsilon} \propto \sigma^8$) and subgrain exponent ($\dot{\varepsilon} \propto \lambda^3$) arise analytically from analysis of the creep data used to develop the model.[41,46] Additionally, it has been shown that for systems where the microstructural features were much finer (< 200 nm) no subgrain formation occurred during creep.[46] It should be noted that dislocation climb remains the operative deformation mechanism during creep even with the change in creep stress exponent from n = 4 to 7 to n = 8 to 10.[41,42]

The steady-state creep rate at 14 and 18 MPa was plotted *vs* Ag_3Sn interparticle spacing at 120 °C and 95 °C for bulk Sn-3.5Ag solder (Figure 2). The results reveal a dependence of strain rate with λ to the power of 3. These results were further validated by normalizing the creep-strain rate by $D\lambda^3$ and plotting this *vs* stress normalized by shear modulus (Figure 3). The data is well described by a slope of ~8, confirming the influence of subgrain formation and diffusion along dislocation cores.

Our hypothesis of subgrain formation controlled by Ag_3Sn particles is further supported by TEM analysis. Figure 4 shows evidence of subgrain formation in Sn-3.5Ag cooled at 24 °C/s. The formation of low-angle boundary networks is readily observed in the crept specimens. The formation of the cell walls is due to accumulation of edge dislocations by climb leading to the development of the subgrain.[47] Some degree of subgrain formation may also be occurring in the 24 °C/s Sn-Cu alloy with n exponents of 10 and 8 observed at 25 °C and 95 °C. However, due to the absence of fine Ag_3Sn particles, and the coarse spacing between Cu_6Sn_5

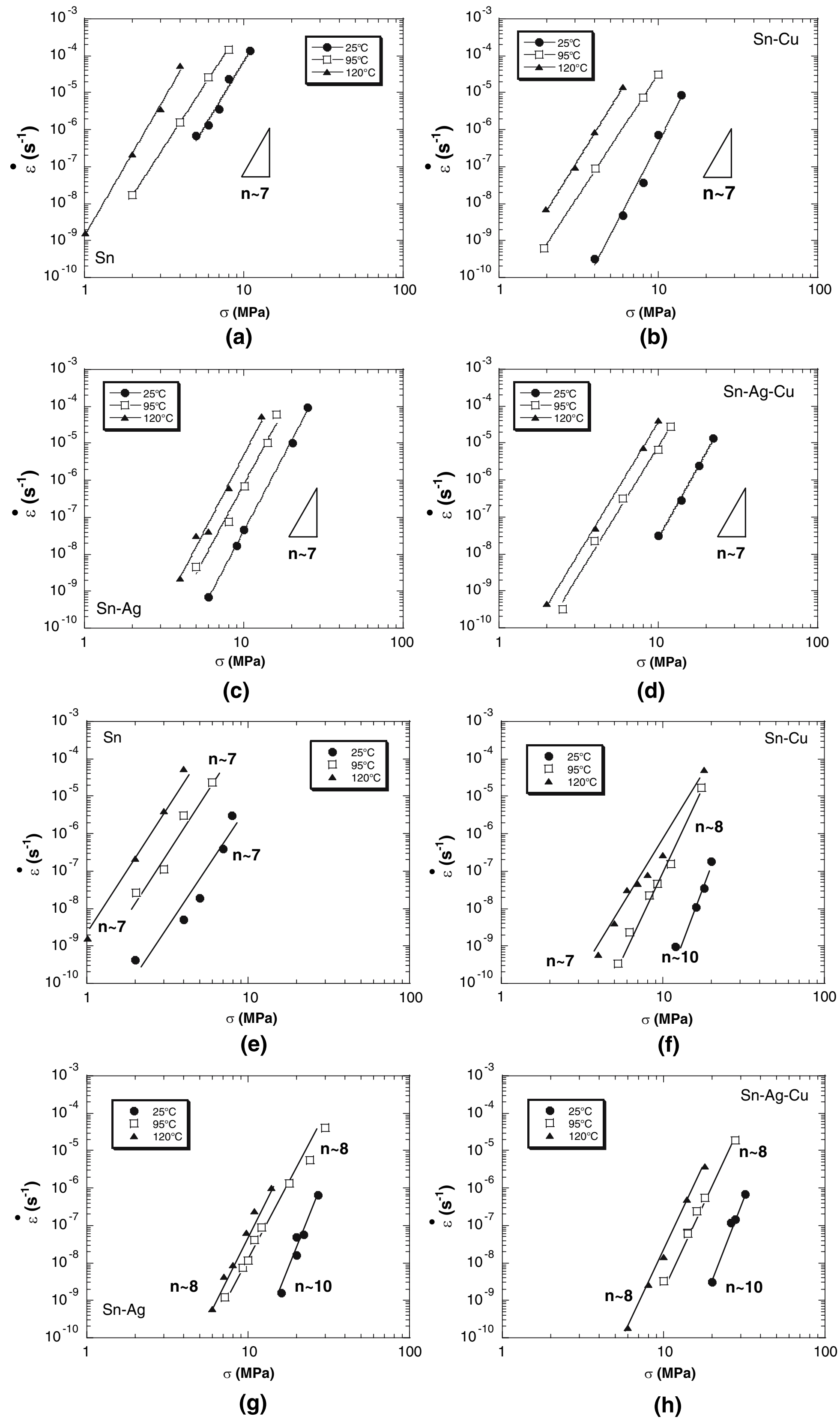

Fig. 1—Steady-state creep rate as a function of stress for alloys cooled at 0.1 °C/s: (*a*) Sn, (*b*) Sn-0.7Cu, (*c*) Sn-3.5Ag, and (*d*) Sn-3.9Ag-0.7Cu; and cooled at 24 °C/s: (*e*) Sn, (*f*) Sn-0.7Cu, (*g*) Sn-3.5Ag, and (*h*) Sn-3.9Ag-0.7Cu.

Table III. Summary of the Stress Exponent for the Respective Solder Systems

	Bulk Solder			
	0.1 °C/s		24 °C/s	
Solder System	25 °C to 120 °C	25 °C	95 °C	120 °C
Sn	7	7	7	7
Sn-Cu	7	10	8	7
Sn-Ag[7]	7	10	8	8
Sn-Ag-Cu	7	10	8	8

Table IV. Activation Energies for Bulk Solder Alloys (0.1 °C /s)

Solder Alloy	25 °C to 120 °C (kJ/mol)
Sn	63.6 ± 3.8
Sn-Cu	56.5 ± 0.5
Sn-Ag[7]	52.8 ± 1.0
Sn-Ag-Cu	60.7 ± 0.3

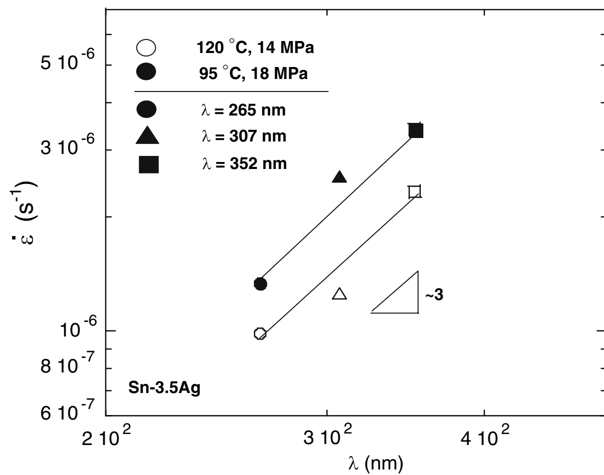

Fig. 2—Creep dependence on subgrain size for bulk Sn-3.5Ag water-cooled at 120 °C, 14 MPa and 95 °C, 18 MPa. The results indicate $\dot{\varepsilon} \propto \lambda^P$, where $p = 3$.

particles (~390 nm) the fraction of subgrain networks is much lower and thus, the observed stress exponent of 7 at 120 °C. In fact, Weertman[48] has shown that the creep rate is controlled by annihilation of piled-up dislocations through climb within grain boundaries, and concluded that in coarse grained materials with subgrain formation the subgrains may not be an effective barrier to piled-up dislocations.

B. *Creep Behavior of Solder/Cu Joint*

The creep behavior of the same alloys in Sn-rich solder/Cu joint form was studied at 25 °C, 60 °C, 95 °C, and 130 °C. Since the solder joints were tested in shear using a lap shear geometry, the creep-strain rate was measured in terms of steady-state shear strain rate, $\dot{\gamma}$, at a given applied shear stress, τ (Figure 5). Table V

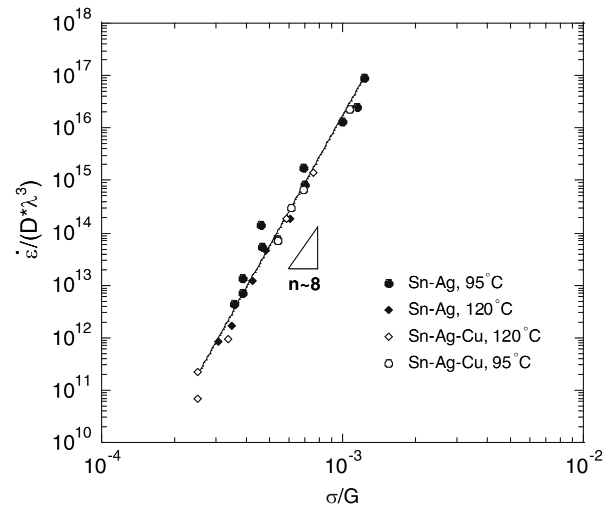

Fig. 3—$\dot{\varepsilon}/D\lambda^3$ *vs* s/G, where l is the subgrain size. Bulk water-cooled creep data superimposed on a common curve attesting to the $\dot{\varepsilon} \propto \lambda^3$ at constant diffusivity and modulus compensated stress. Slope of the curve reveals that the stress exponent is ~8.

summarizes the creep-stress exponents for the Sn-rich solder/Cu joints. The Sn-3.5Ag and Sn-3.9Ag-0.7Cu solder/Cu joints (Figure 5(a) and (b)) both exhibit classic dispersion-strengthened creep behavior. A well-defined two-tiered behavior comprised of a low-stress regime (LSR) and high-stress regime (HSR) is quite apparent. In the LSR, a stress exponent (n) of approximately 6 was observed at 25 °C and 60 °C, while at 95 °C and 130 °C n was approximately equal to 4. These exponents are characteristic of creep controlled by dislocation climb.[49] In the HSR, the stress exponent was always greater than 10. The observed change in the stress exponent between low temperatures (25 °C and 60 °C) and high temperatures (95 °C and 130 °C) can be linked to a change in diffusion mechanism during creep. The Sn and Sn-0.7Cu joints (Figure 5(c) and (d)), on the other hand, exhibit a single-tier behavior at low temperatures and an "S-shaped" transition at high temperatures, analogous to Newtonian viscous glide at grain boundaries.[50] The absence of a transition in stress exponent behavior between the LSR and HSR is expected, since the Sn is a single phase material and the Sn-0.7Cu solder joints show little dispersion strengthening, due to the large Cu_6Sn_5 intermetallic particles and their large spacing.

The Sn and Sn-0.7Cu solder joints also both exhibited a single-tiered stress dependence, indicating a single creep mechanism. This was also apparent upon examining the activation energy measurements for the entire temperature range (25 °C to 130 °C) studied (Table VI). A single diffusion mechanism was identified and it correlates to lattice diffusion in pure Sn, which has been reported to range between 98 to 118 kJ/mol.[36,37,38] The difference in diffusion mechanisms observed between bulk specimens and small solder/Cu joints in Sn and Sn-0.7Cu may be attributed to the lack of subgrain formation at the smaller grain sizes of the solder joint, and thus, less of a dependence of diffusion along

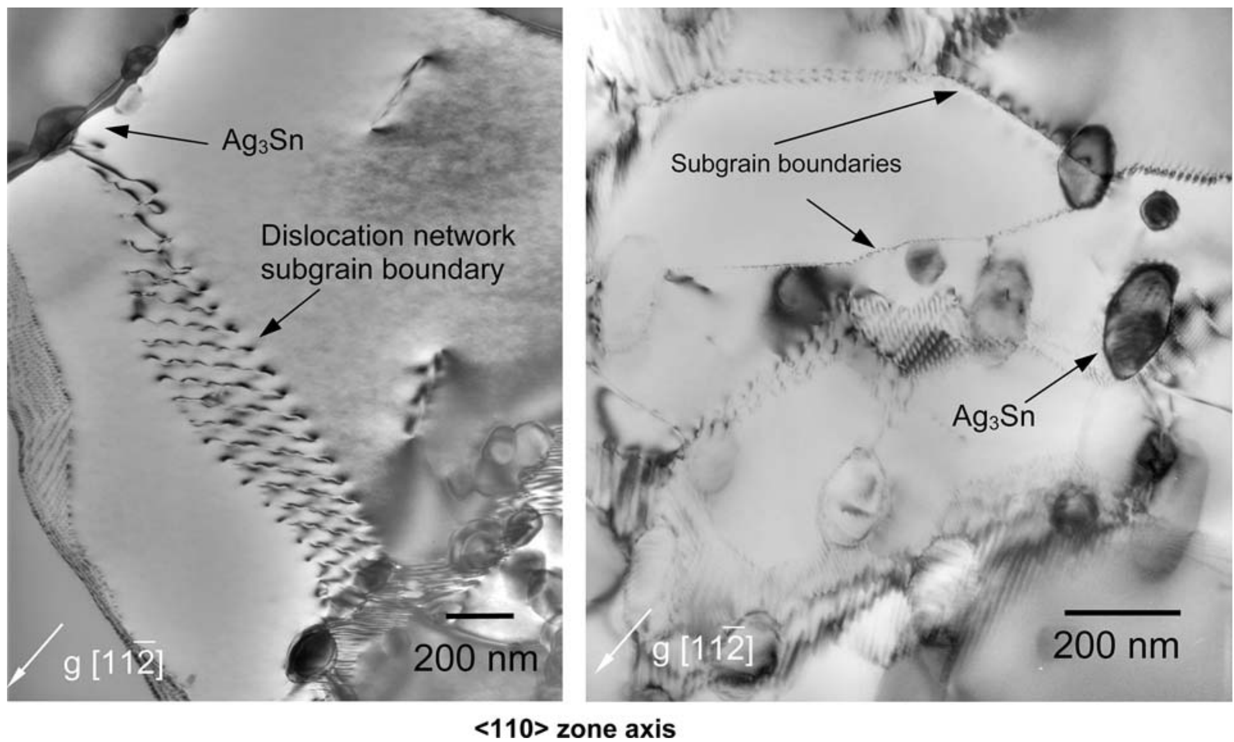

Fig. 4—Evidence of subgrain boundary formation during creep deformation in water-cooled Sn-3.5Ag solder at 12 MPa and 95°C.

dislocation cores. Transitions in creep mechanisms with grain size have also been observed in other material systems.[51–56]

The creep behavior of Sn-Ag-Cu and Sn-Ag solder joints is intimately linked to their dispersion-strengthened microstructures, and is inherently different from both the bulk alloys, and the Sn and Sn-0.7Cu solder joints. Two activation energies were measured in two temperature regimes, indicating that two different diffusion mechanisms are operating during creep. For the higher temperature regime (95 °C to 130 °C), the activation energies for both Sn-3.5Ag and Sn-3.9Ag-0.7Cu fall between 105 and 126 kJ/mol. These compare well with the activation energies for lattice diffusion of pure Sn.[36,37,38] In the lower temperature regime (25 °C to 95 °C), the activation energy for both Sn-3.5Ag and Sn-3.9Ag-0.7Cu is approximately 0.4 to 0.5 of the value for lattice diffusion of pure Sn, and has been confirmed to correspond to dislocation core diffusion.[37,57] Work conducted by Breen and Weertman[38] on polycrystalline Sn showed that the transition temperature from lattice diffusion to dislocation core diffusion occurs abruptly in a temperature range of 0.7 to 0.85 T_m. This has been confirmed in both the present study for Sn-3.9Ag-0.7Cu and in the work by Kerr and Chawla[21] for Sn-3.5Ag.

The transition in activation energy can be used to explain the change in stress exponent observed between the low-temperature regime ($n = \sim 4$) to the high-temperature regime ($n = \sim 6$). Sherby and Burke[58] suggested that during high-temperature creep, both lattice diffusion and dislocation core diffusion are taking place simultaneously. A relationship for creep considering an effective diffusion coefficient, D_{eff}, was developed:

$$D_{\text{eff}} = D_l f_l + D_d f_d \qquad [3]$$

$$f_d = n/N\rho \qquad [4]$$

where D_l is the lattice diffusion coefficient, D_d is the dislocation core diffusion coefficient, and f_l and f_d are the fraction of atoms associated with lattice diffusion and dislocation core diffusion, respectively. The fraction of atoms participating in a given diffusion mechanism (f_d), is expressed in terms of the number of contributing atoms (n), number of atoms per m^2 (N), and the dislocation density (ρ).[57] The dislocation density then can be expressed as a function of stress:

$$\rho = K\left(\frac{\sigma}{E}\right)^2 \qquad [5]$$

where K is a constant, σ is the applied stress, and E is Young's modulus of the material. Using Eq. [5], f_d can be expressed in terms of stress.[59] When D_{eff} is substituted into the constitutive equation for creep, we obtain the following relation:

$$\begin{aligned}\dot{\gamma} &= A\left(\frac{D_{\text{effective}}G\mathbf{b}}{kT}\right)\left(\frac{\sigma}{G}\right)^n = A'(D_{\text{effective}})\left(\frac{\sigma}{G}\right)^n \\ &= A'(D_{\text{core}})\left(\frac{\sigma}{G}\right)^2\left(\frac{\sigma}{G}\right)^n = A'(D_{\text{core}})\left(\frac{\sigma}{G}\right)^{n+2} \qquad (6)\end{aligned}$$

Thus, assuming that diffusion takes place primarily along dislocation cores in the lower temperature regime, the dependence of strain rate on stress will increase by a power of 2.

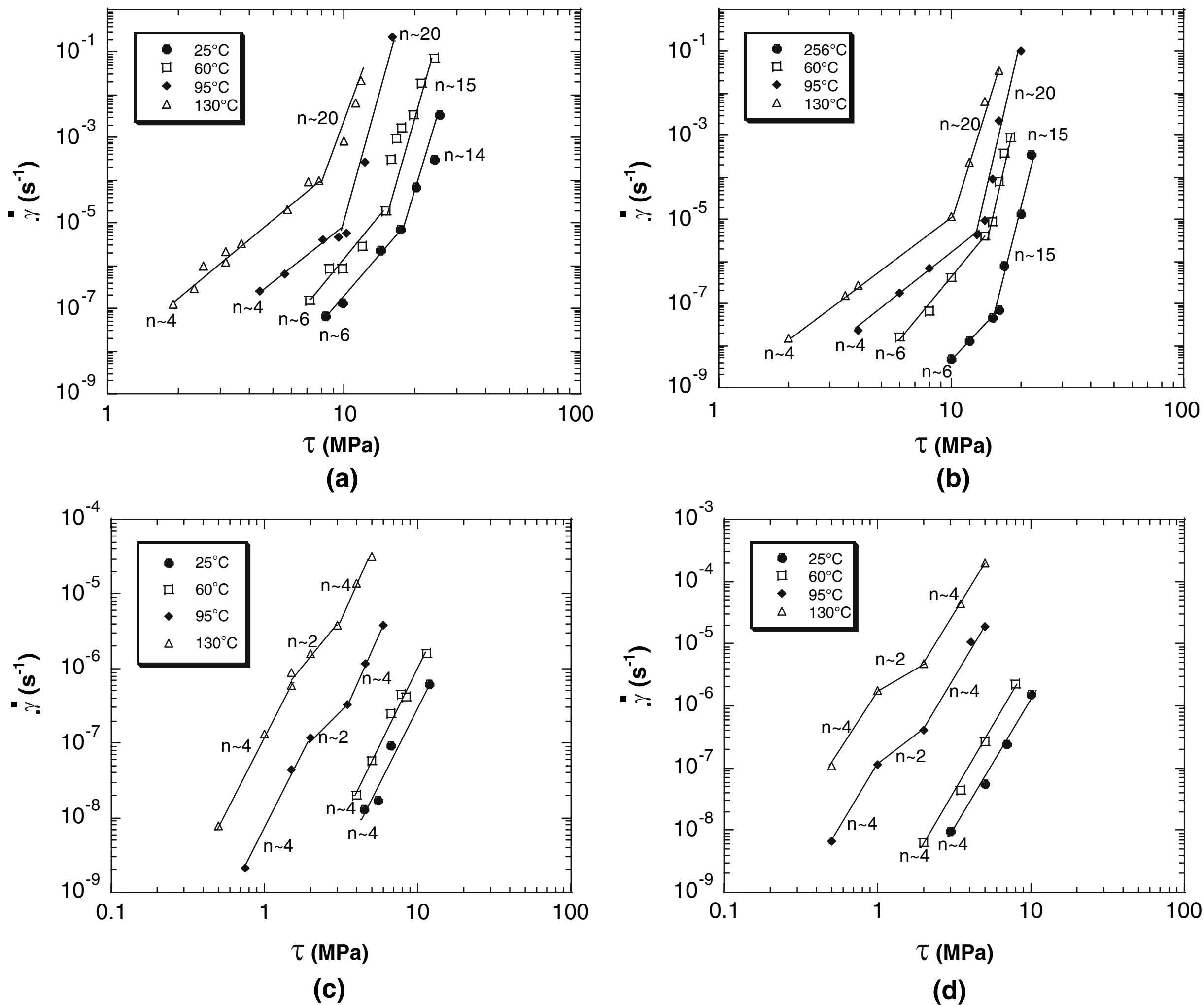

Fig. 5—Strain rate *vs* applied stress for (*a*) Sn-3.5Ag[32] and (*b*) Sn-3.9Ag-0.7Cu solder joints at 25 °C, 60 °C, 95 °C, and 130 °C. Note the transition in stress exponent from 6 to 4 in the low-stress regime with increasing temperature. Strain rate *vs* applied stress for (*c*) Sn and (*d*) Sn-0.7Cu solder joints at 25 °C, 60 °C, 95 °C, and 130 °C. Note the S-shaped transition in the high-temperature regime (95 °C to 130 °C).

Table V. Summary of the Stress Exponent for the Respective Solder Systems

	Solder/Cu Joints			
	LSR		HSR	
Solder System	25 °C to 60 °C	95 °C to 120 °C	25 °C to 60 °C	95 °C to 120 °C
Sn	4		4	
Sn-Cu	4		4	
Sn-Ag[32]	6	4	14 to 15	20
Sn-Ag-Cu	6	4	15	20

Table VI. Activation Energies for Solder Joints in the Low-Stress Regime

	Solder/Cu Joints (kJ/mol)	
Solder System	25 °C to 60 °C	95 °C to 130 °C
Sn	109 ± 6	
Sn-Cu	102 ± 4	
Sn-Ag[21]	50 ± 5	126 ± 8
Sn-Ag-Cu	55 ± 4	105 ± 7

It can be seen that the creep behavior between the bulk and solder joints is notably different. For Sn-Ag and Sn-Ag-Cu alloys in bulk form, a single high-stress exponent defines the data, while for the solder joints a two-tiered behavior is observed (LSR and HSR).

The stress exponent values for the Ag_3Sn-containing solder joint alloys (Sn-Ag and Sn-Ag-Cu) are much higher in the HSR compared to the LSR (Table V). The high-stress exponents in the HSR are consistent with the behavior of many precipitation- and dispersion-strengthened materials where a transition in creep deformation mechanisms is observed.[60–62] In these materials, a fine distribution of second-phase particles exerts a resistive force on dislocations, also termed an internal stress. Thus, the actual creep-stress is equal to the applied stress minus the internal resisting stress. Several studies have invoked the concept of threshold stress in precipitation

and dispersion-strengthened alloys to explain the high apparent stress exponent values and high apparent values for activation energy.[60–63] Other studies have used the threshold stress analysis to study the creep behavior of Sn-rich solders.[8,63] We have used this approach to determine the true stress exponent in the solder systems and to explain the mechanisms that are occurring during creep deformation.

The threshold stress, τ_{th}, can be incorporated into the Mukherjee–Bird–Dorn equation by subtracting it from the applied stress. The expression for the steady-state shear strain rate then becomes

$$\dot{\gamma}_S = A\left(\frac{G\mathbf{b}}{RT}\right)\left(\frac{\tau - \tau_{th}}{G}\right)^n \exp\left(\frac{-Q_c}{RT}\right) \qquad [7]$$

The threshold stress for the creep data was calculated using the following approach. The creep data was analyzed by plotting $\dot{\gamma}_s^{\frac{1}{n}}$ *vs* applied shear stress for n values ranging between 4 and 6 in the LSR. For 25 °C and 60 °C, an exponent of $n = 6$ was applied and for 95 °C and 130 °C, $n = 4$ was used. The curves were then extrapolated to a zero strain rate and the threshold stresses were determined.[60–62] Figure 6 shows a representative plot of the threshold stress analysis, analyzed for Sn-Ag-Cu joints. It should be noted that upon normalizing the applied stress by the temperature-dependant shear modulus, the threshold stress for all temperatures is fairly constant, indicating that the mechanism responsible for the threshold stress is similar at all temperatures.

Several mechanisms have been proposed to explain the origin and magnitude of the threshold stresses in precipitate and dispersion-strengthened alloys, where dislocation mobility is hindered by an array of particles. If dislocations bow out between particles, the threshold stress is equal to the Orowan stress, τ_o, which is given by[64,65]

$$\tau_o = 0.84\left(\frac{G\mathbf{b}}{\lambda - d_P}\right) \qquad [8]$$

Second, the internal stress may be equal to the dissociation stress, τ_D, which describes the stress associated

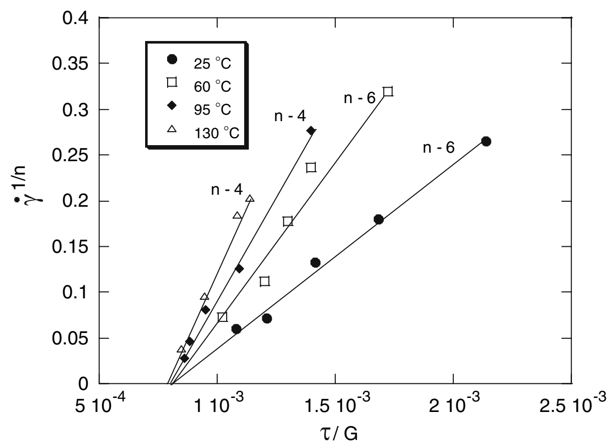

Fig. 6—Threshold stress for Sn-3.9Ag-0.7Cu solder joint.

with the dissociation of lattice dislocations into interfacial dislocations at the matrix-particle interface that surmount the particle by climb:[66]

$$\tau_D = 10^{-3}\left(\frac{G\mathbf{b}}{r_P}\right)\exp\left(\frac{20 r_P}{\lambda}\right) \qquad [9]$$

Third, if a back stress, τ_B, is required to create an additional segment of dislocation as it surmounts the particle by local climb, the threshold stress is given by[67,68]

$$\tau_B = 0.3\left(\frac{G\mathbf{b}}{\lambda}\right) \qquad [10]$$

where λ is the interparticle spacing, d_P is the average particle size, r_P is the average particle radius, G is the shear modulus, and $\mathbf{b}$ is burger's vector (0.317 nm for Sn[68,69]). A fourth mechanism has been observed experimentally that elucidates the secondary interactions of the dislocation with the particles after the dislocation has surmounted the particle.[70–72] Initially, the dislocation line length in close proximity to the particle-matrix interface undergoes climb, while the portion not in contact with the particle remains in the glide plane. It is suggested that the particles have interfaces that may slip and can attract dislocations by reducing the total elastic strain energy. The attractive interaction results in the dislocation detaching from the departure side and results in a detachment stress that reflects the increase in strain energy of the dislocation. Arzt and co-workers[39,73,74] developed the following model to analyze the detachment process:

$$\tau_d = \left(\frac{G\mathbf{b}}{\lambda}\right)\sqrt{(1 - k^2)} \qquad [11]$$

where λ is the interparticle spacing, G is the shear modulus, $\mathbf{b}$ is burger's vector, and k is the relaxation

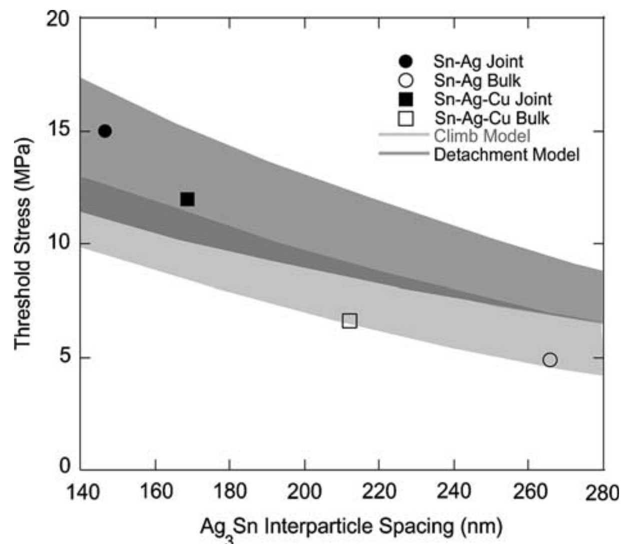

Fig. 7—Comparison of predicted threshold stress determined by dislocation climb and detachment models with experimentally determined threshold stress as a function of interparticle spacing.

parameter described by a modified dislocation line energy:

$$\left(G\mathbf{b}^2\right)_p = k\left(G\mathbf{b}^2\right)_m \qquad [12]$$

where p refers to the particle interface and m the matrix. Arzt and Wilkinson[73] showed that the relaxation parameter, k, also provides a critical transition value below which dislocation bypass becomes detachment-controlled.

The model predictions were compared to the experimentally determined threshold stress. A comparison was only made on materials with a fine microstructure since these materials exhibited classical dispersion strengthening behavior, *i.e.*, anomalously high values of creep-stress exponent. Kerr and Chawla[32] initially suggested that the high-stress regime was caused by Orowan bowing of dislocations around the Ag_3Sn particles. However, upon comparing the model predictions to our experimental results it is evident that local climb and detachment model predict the experimental threshold stress best, suggesting dislocation climb over the intermetallic particles as the principal creep mechanism. Therefore, it appears that at larger Ag_3Sn interparticle spacing the creep behavior is dominated by dislocation climb, and as the interparticle spacing

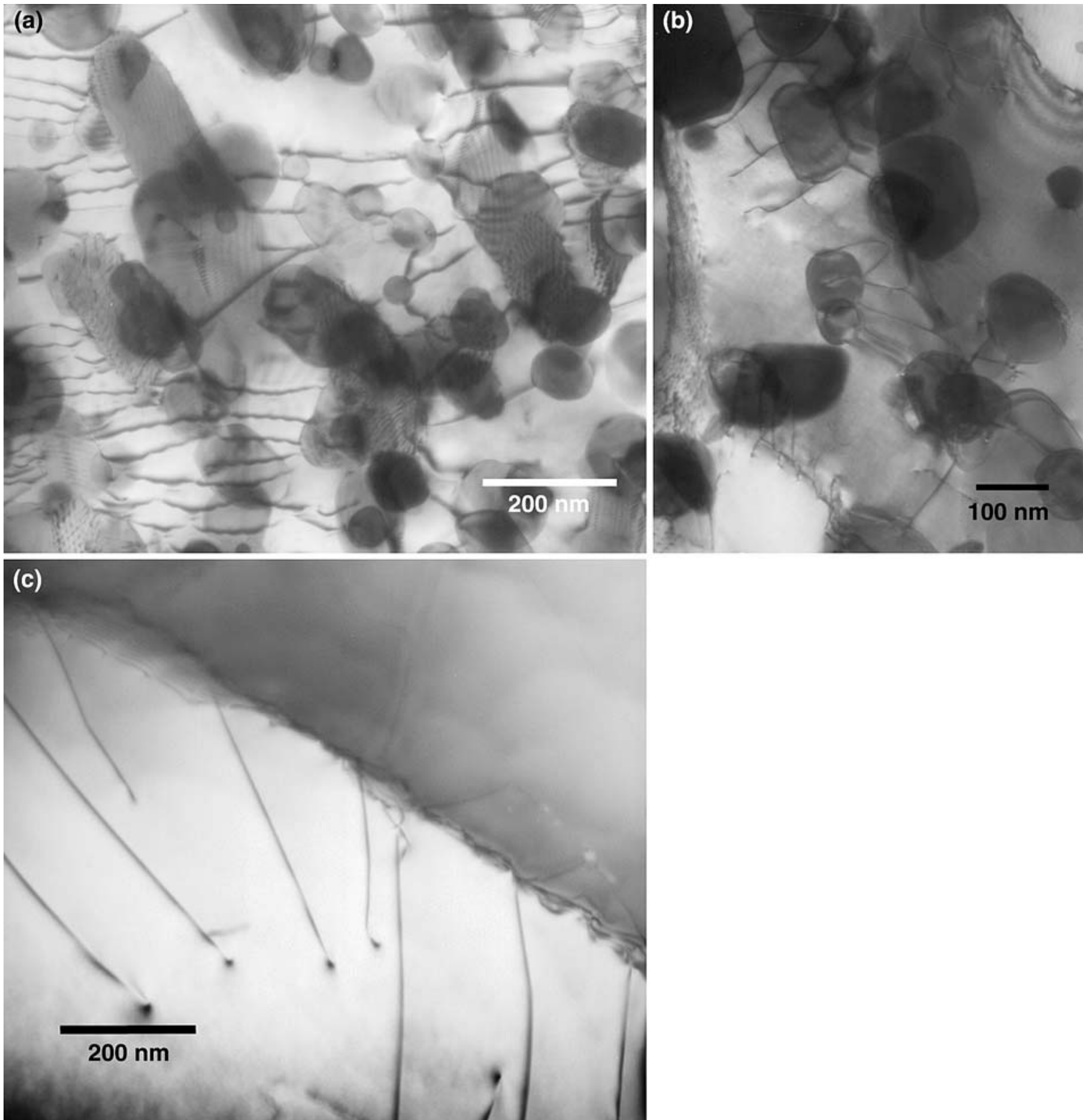

Fig. 8—TEM micrographs after creep (⟨110⟩ zone axis): (*a*) eutectic region within a Sn-3.9Ag-0.7Cu sample crept at 14 MPa and 95 °C showing dislocation-particle interaction, (*b*) eutectic region within Sn-3.5Ag sample crept at 12 MPa and 95 °C showing similar interactions, and (*c*) grain boundary of a Sn sample crept at 4 MPa and 95 °C showing dislocation mobility is unrestricted with lack of impeding particles.

decreases this is transitioned to climb controlled by dislocation detachment (Figure 7).

Local climb and detachment conclusions are further supported by TEM analysis of the crept samples (Figure 8(a) and (b)). These micrographs show dislocations interacting with the particles and likely climbing over Ag_3Sn. Thus, dislocation climb appears to be the operative mechanism in the precipitate-strengthened Sn-3.9Ag-0.7Cu and Sn-3.5Ag solder/Cu joints. It is evident that dislocation mobility is severely hindered by interaction with the finely dispersed intermetallic particles. This is very different from the case of pure Sn, where the dislocations move unobstructed (Figure 8(c)). The preceding analysis indicates that the creep behavior of the dispersion-strengthened alloys, Sn-Ag and Sn-Ag-Cu, appears to be controlled by Ag_3Sn size and spacing. To examine the effect of interparticle spacing, creep experiments were conducted on Sn-3.5Ag solder joints of different Ag_3Sn size and spacing (as controlled by cooling rate).

The data are shown in Figure 9. The plot clearly shows that for the lower interparticle spacing of Ag_3Sn, the creep behavior is described by a two-tier transition in the stress exponent. Thus, we can deduce that the single-tier behavior observed in bulk specimens is due to the coarser microstructure in these materials, *i.e.*, larger Ag_3Sn size and spacing. The Ag_3Sn particle size in the bulk tensile specimens was approximately 70 pct larger than that of the other microstructures, while the interparticle spacing was approximately 56 pct larger. It is likely that a critical particle size and spacing exists, and it corresponds to the transition between single-tiered and the two-tiered creep behavior.

C. *Finite-Element Modeling of Grain-Boundary Sliding Accommodated by Power-Law Creep*

It is interesting to note that in pure Sn and Sn-0.7Cu solder joints at 95 °C and 130 °C, a transition region at intermediate stresses is observed. As discussed previously, in both the LSR and HSR the stress exponent is approximately 4. This S-shaped behavior was first observed by Cline and Alden[50] for Pb-Sn eutectic alloys. They reported that metallographic observations show increasing grain boundary offsets with decreasing strain rate near the upper strain rate end of the ''transition.''

To better understand the deformation modes present we invoke the model and explanation provided by Crossman and Ashby.[75] They modeled the transition in systems where the boundaries between grains are allowed to slide in a Newtonian viscous manner, and deformation within the grains takes place by power-law creep. At low stress, deformation within the grains is accommodated by sliding at the grain boundaries so there is acceleration in creep rate. Increasing the stress results in a transition in creep rate, where the contribution of dislocation creep increases. Finally, at stress levels beyond the transition, the contribution from free sliding to the overall deformation is negligible. The net effect is that a stress dependence of $n = \sim 4$ exists in both the low- and high-stress regimes.

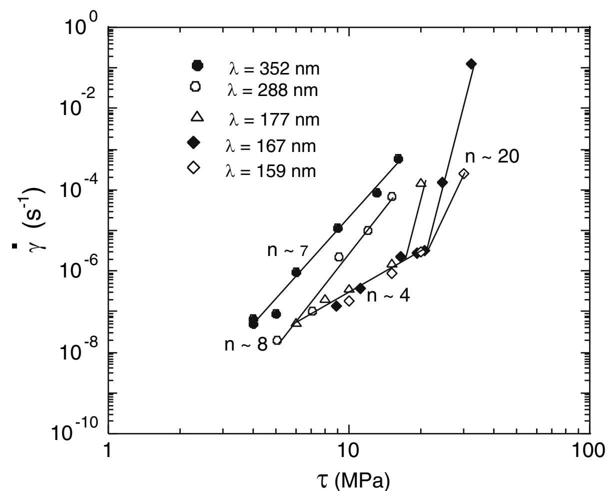

Fig. 9—Comparison of the Sn-3.5Ag creep data at 95 °C for all testing geometries. For a relatively constant interparticle spacing, the creep behavior is similar irrespective of testing geometry.

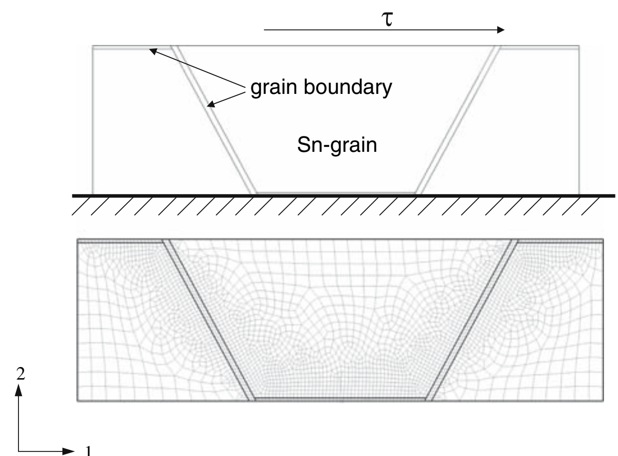

Fig. 10—Schematic and finite element method model of hexagonal Sn grains with viscous grain boundaries used to model creep behavior in pure Sn and Sn-Cu alloy.

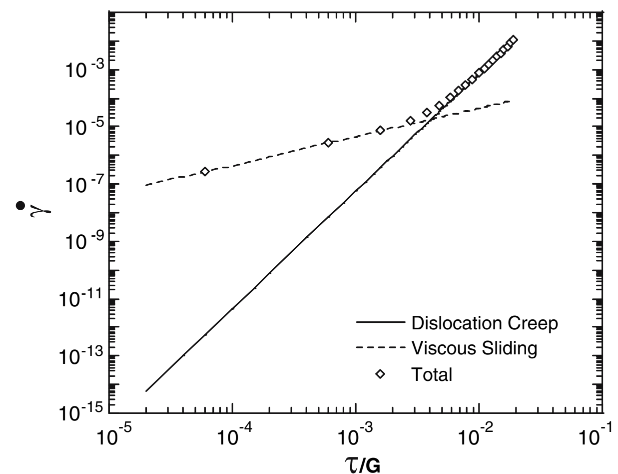

Fig. 11—Constitutive behavior for the viscous Sn grain boundary model in Fig. 9.

To better understand the deformation modes present in the solder joints, we conducted finite element modeling based on the model developed by Crossman and Ashby.[75] A two-dimensional, plane strain, axisymmetric model of hexagonal grains encompassed by a viscous boundary layer was used to analyze the stress state of the system. The symmetry axis was fixed vertically (displacement in the 2-direction with $U_2 = 0$) but was allowed to move horizontally while the bottom of sample was fixed ($U_2 = 0$ and displacement in the 1-direction, U_1, is 0). Figure 10 shows a schematic of the modeled grains, which were loaded in shear.

The boundaries between grains were allowed to slide in a Newtonian viscous manner, and deformation within the grains was modeled using power-law creep:

$$\dot{\gamma} = A\left(\frac{D_V G\mathbf{b}}{\mathrm{R}T}\right)\left(\frac{\tau}{G}\right)^n \qquad [13]$$

where G is the shear modulus, $\mathbf{b}$ is the burger's vector, D_V is the lattice diffusion, R is the gas constant, and n is the stress exponent. The relative sliding rate of two grains that meet at such a boundary is given by

$$\dot{U}_{GB} = \left(\frac{w}{\eta_B}\right)\tau \qquad [14]$$

where w is defined as twice the atomic size, which slides in a Newtonian viscous manner, and η_b is the viscosity of the boundary, defined as

$$\eta_B = \left(\frac{\mathrm{k}T}{8\mathbf{b}D_B}\right) \qquad [15]$$

where D_B is the grain boundary diffusion coefficient. The constitutive behavior for the grain boundary is shown in Figure 11. At low stress, deformation within the grains is accommodated by sliding at the grain boundaries. Thus, an acceleration in creep rate is observed. Increasing stress results in a transition in creep rate, whereby the contribution of dislocation creep increases. Finally, at stress levels beyond the transition, the contribution

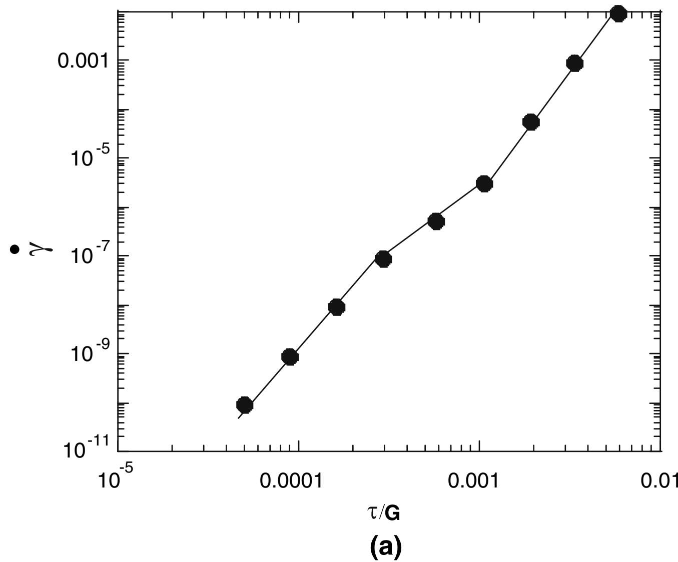

Fig. 12—(*a*) Finite element model prediction of S-shaped creep behavior observed experimentally in pure Sn and Sn-Cu at elevated temperatures. (*b*) Stress state within Sn grain and grain boundary during deformation.

from free sliding to the overall deformation is negligible. The finite element method (FEM) model was able to predict the S-shaped creep behavior inherent in pure Sn/Cu joints (Figure 12(a)). Figure 12(b) shows the predicted stress state within the grain structure during deformation. The viscous nature of the boundary accommodation results in relaxation of the stress within the boundary. The net effect is that a stress dependence of $n = \sim 4$ exists at both low and high stresses, even though the strain rates are somewhat accelerated within the low-stress regime

IV. CONCLUSIONS

The creep behavior of Sn-rich bulk solders and small solder joints was investigated. Based on experimental and modeling results, the following conclusions are made.

1. The creep behavior of the bulk solder alloys was controlled by subgrain formation of dislocations pinned by Ag_3Sn particles (in Sn-Ag and Sn-Ag-Cu) or Cu_6Sn_5 and grain boundaries (Sn-Cu and Sn). The creep-stress exponents observed for these materials systems ($n = \sim 7$ to 8) and TEM observations support this conclusion. Activation energies in these materials correlated with that of diffusion along dislocation cores (at subgrain boundaries) in Sn.
2. The Sn-3.5Ag and Sn-3.9Ag-0.7Cu solder joints behave as precipitation strengthened systems. In these solder alloys, the intermetallic particles strengthen the Sn matrix, and the creep behavior in both systems show a low-temperature regime (25 °C to 60 °C) where $n = 6$, and high-temperature regime (95 °C to 130 °C) where $n = 4$. This phenomenon can be explained by the measured transition in the activation energy, where dislocation core diffusion transitions to lattice diffusion at higher temperatures.
3. Local climb and dislocation detachment have been established as the operative mechanisms responsible for the observed threshold stress in the Sn-Ag and Sn-Ag-Cu solder joints. This is based on the threshold stress dependence of Ag_3Sn interparticle spacing and good agreement with analytical predictions.
4. It was established that the creep behavior of pure Sn and Sn-0.7Cu solder joints is different from precipitation-strengthened systems. The creep data points to a single tier stress exponent ($n = 4$), which is consistent with the lattice diffusion of Sn. However, at high temperatures both solder systems show an S-shaped phenomenon, corresponding to power-law creep accommodated by viscous grain boundary sliding. The experimentally observed behavior was modeled and confirmed by finite element analysis.

ACKNOWLEDGMENTS

The authors gratefully acknowledge financial support for this research from the National Science Foundation under contract #DMR-0092530 (Drs. H. Chopra, S. Ankem, B. Macdonald, and K.L. Murty, program managers).

REFERENCES

1. W.J. Plumbridge, C.R. Gagg, and S. Peters: *J. Electron. Mater.*, 2001, vol. 30, pp. 1178–83.
2. J. Glazer: *Int. Mater. Rev.*, 1995, vol. 40, pp. 65–93.
3. J.W. Jang, A.P. De Silva , T.Y. Lee, J.K. Lee, and D.R. Frear: *Appl. Phys. Lett.*, 2001, vol. 79, pp. 482–84.
4. S.K. Kang and A.K. Sarkhel: *JEM*, 1994, vol. 23, pp. 701–07.
5. K.J. Puttlitz and K.A. Stalter: *Handbook of Lead-Free Solder Technology for Microelectronic Assemblies*, Marcel Dekker Inc., New York, NY, 2004.
6. R.S. Sidhu and N. Chawla: *Metall. Mater. Trans. A*, 2007, vol. 38A. doi: 10.1007/s11661-007-9414-0.
7. F. Ochoa, X. Deng, and N. Chawla: *J. Electron. Mater.*, 2004, vol. 33, pp. 1596–607.
8. C.M.L. Wu and M.L. Huang: *J. Electron. Mater.*, 2002, vol. 31, pp. 442–48.
9. M.D. Mathew, H. Yang, S. Movva, and K.L. Murty: *Metall. Mater. Trans. A*, 2005, vol. 36, pp. 99–105.
10. H. Mavoori, J. Chin, S. Vaynman, B. Morgan, L. Keer, and M. Fine: *J. Electron. Mater.*, 1997, vol. 26, pp. 783–90.
11. K. Wu, N. Wade, J. Cui, and K. Miyahara: *J. Electron. Mater.*, 2003, vol. 32, pp. 5–8.
12. R.J. McCabe and M.E. Fine: *Metall. Mater. Trans. A*, 2002, vol. 33, pp. 1531–39.
13. P.T. Vianco, J.A. Rejent, and A.C. Kilgo: *J. Electron. Mater.*, 2004, vol. 33, pp. 1389–1400.
14. P.T. Vianco, J.A. Rejent, and A.C Kilgo: *J. Electron. Mater.*, 2004, vol. 33, pp. 1473–84.
15. Q. Xiao and W.D. Armstrong: *J. Electron. Mater.*, 2005, vol. 34, pp. 196–211.
16. N. Wade, K. Wu, J. Kunii, S. Yamada, and K. Miyahara: *J. Electron. Mater.*, 2001, vol. 30, pp. 1228–31.
17. D.K. Joo, J. Yu, and S.W. Shin: *J. Electron. Mater.*, 2003, vol. 32, pp. 541–47.
18. M.M. El-Bahay, M.E. El Mossalamy, M. Mahdy, and A.A. Bahga: *J. Mater. Sci.-Mater. Electron.*, 2004, vol. 15, pp. 519–26.
19. Y. Kariya, T. Asai, and T. Suga: *Proc. SPIE*, 2004, vol. 5852, pp. 297–301.
20. C.H. Raeder, G.D. Schmeelk, D. Mitlin, T. Barbieri, W. Yang, L.F. Felton, R.W. Messler, D.B. Knorr, and D. Lee: *IEEE CPMT Int. Electronic Manufacturing Technology Symp.*, pp. 1–6.
21. M. Kerr and N. Chawla: *JOM*, 2004, vol. 56, pp. 50–54.
22. H. Rhee, F. Guo, J.G. Lee, K.C. Chen, and K.N. Subramanian: *J. Electron. Mater.*, 2003, vol. 32, pp. 1257–64.
23. S.G. Jadhav, T.R. Bieler, K.N. Subramanian, and J.P. Lucas: *J. Electron. Mater.*, 2001, vol. 30, pp. 1197–1205.
24. J.H. Lau, S.H. Pan, and C. Chang: *J. Electron. Packaging*, 2002, vol. 124, pp. 69–76.
25. H.G. Song, J.W. Morris, Jr., and F. Hua: *JOM*, 2002, vol. 56, pp. 30–32.
26. S.W. Shin and J. Yu: *J. Electron. Mater.*, 2005, vol. 34, pp. 188–95.
27. R. Darveaux and K. Banerji: *IEEE Trans. Compon. Hybr.*, 1992, vol. 15, pp. 1013–24.
28. S. Wiese and K.J. Wolter: *Microeletron. Rel.*, 2004, vol. 44, pp. 1923–31.
29. Z. Chen, Y. Shi, and Z. Xia: *J. Electron. Mater.*, 2004, vol. 33, pp. 964–71.
30. F. Guo, S. Choi, J.P. Lucas, and K.N. Subramanian: *J. Electron. Mater.*, 2000, vol. 29, pp. 1241–48.
31. MTS Systems Corp., http://www.mts.com.
32. M. Kerr and N. Chawla: *Acta Mater.*, 2004, vol. 52, pp. 4527–35.
33. F. Garofalo: *Fundamentals of Creep and Creep-Rupture in Metals*, Macmillan, New York, NY, 1965, pp. 66–69.
34. R.W. Evans and B. Wilshire: *Introduction to Creep*, The Institute of Materials, London, 1993, p. 46.
35. A.K. Mukherjee, J.E. Bird, and J.E. Dorn: *Trans. ASM*, 1969, vol. 62, pp. 155–69.
36. F.A. Mohamed, K.L. Murty, and J.W. Morris, Jr.: *Metall. Trans.*, 1973, vol. 4, pp. 935–40.

37. S. Suh, J.B. Cohen, and J. Weertmen: *Metall. Trans. A*, 1983, vol. 14A, pp. 117–26.
38. J.E. Breen and J. Weertman: *Trans. AIME*, 1955, vol. 203, pp. 1230–34.
39. E. Arzt and J. Rosler: *Acta. Metall. Mater.*, 1988, vol. 36, pp. 1053–60.
40. O.D. Sherby, R.H. Klundt, and A.K. Miller: *Metall. Trans. A*, 1977, vol. 8A, pp. 843–50.
41. J. Lin and O.D. Sherby: *Res. Mechanica*, 1981, vol. 2, pp. 251–93.
42. O.D. Sherby and E.M. Taleff: *Mater. Sci. Eng. A*, 2002, vol. 322, pp. 89–99.
43. S.L. Robinson and O.D. Sherby: *Acta Metall.*, 1969, vol. 17, pp. 109–25.
44. I.S. Servi and N.J. Grant: *Trans. AIME*, 1951, vol. 191, p. 917.
45. J.L. Lytton, C.R. Barrett, and O.D. Sherby: *Trans. TMS-AIME*, 1965, vol. 233, p. 1399.
46. R.S. Mishra and A.B. Pandey: *Metall. Trans. A*, 1990, vol. 21A, pp. 2089–90.
47. W.A. Wood and G.R. Wilms: *J. Inst. Met.*, 1948–49, vol. 75, p. 613.
48. J. Weertman: in *Rate Process in Plastic Deformation of Materials*, J.C.M. Li and A.K. Mukherjee, eds., ASM, Metals Park, OH, 1975, p. 315.
49. R. Lagneborg and B. Bergman: *Met. Sci.*, 1976, vol. 10, pp. 20–28.
50. H.E. Cline and T.H. Alden: *Trans. AIME*, 1967, vol. 239, pp. 710–14.
51. G. Malakondaiah and P.R. Rao: *Met. Sci.*, 1981, vol. 15, pp. 442–46.
52. B. Wilshire and C.J. Palmer: *Scripta Mater.*, 2002, vol. 46, pp. 483–88.
53. S.V. Raj: *Mater. Sci. Eng.*, 1987, vol. 96, pp. 57–64.
54. G. Malakondaiah and P.R. Rao: *Acta Metall.*, 1981, vol. 29, pp. 1263–75.
55. W.L. Bradley, J.S. August, and D.K. Matlock: *Met. Sci.*, 1977, vol. 11, pp. 168–70.
56. Z.A. Yang, Z.G. Wang, and S.Q. Wang: *Mater. Sci. Eng. A*, 1988, vol. 102, pp. 17–23.
57. H. Luthy, A.K. Miller, and O.D. Sherby: *Acta Metall.*, 1980, vol. 28, pp. 169–78.
58. O.D. Sherby and P.M. Burke: *Prog. Mater. Sci.*, 1967, vol. 1, p. 325.
59. O.A. Ruano, A.K. Miller, and O.D. Sherby: *Mater. Sci. Eng.*, 1981, vol. 51, pp. 9–16.
60. J. Cadek: *Mater. Sci. Eng.*, 1987, vol. 94, pp. 79–92.
61. J. Cadek and K. Milicka: *Scripta. Mater.*, 1997, vol. 37, pp. 1039–44.
62. S. Spigarelli, E. Cerri, P. Bianchi, and E. Evangelista: *Mater. Sci. Technol.*, 1999, vol. 15, pp. 1433–40.
63. S. Wiese, F. Feustel, and E. Meusel: *Sens. Actuators A-Phys.*, 2002, vol. 99, pp. 188–93.
64. E. Orowan: in *Dislocations in Metals*, M. Cohen, ed., AIME, New York, NY, 1954, p. 131.
65. U.F. Kocks: *Phil. Mag.*, 1966, vol. 13, pp. 541–66.
66. R.S. Mishra, T.K. Nandy, and G.W. Greenwood: *Phil. Mag. A*, 1994, vol. 69, pp. 1097–109.
67. R.S.W. Shewfelt and L.M. Brown: *Phil. Mag.*, 1977, vol. 35, pp. 945–62.
68. E. Arzt and M.F. Ashby: *Scripta Metall.*, 1982, vol. 16, pp. 1285–90.
69. J. Rosler and E. Arzt: *Acta Metall. Mater.*, 1990, vol. 38, pp. 671–83.
70. V.C. Nardone and J.K. Tien: *Scripta Mater.*, 1983, vol. 17, pp. 467–70.
71. J.H. Schroder and E. Arzt: *Scripta Mater.*, 1985, vol. 19, pp. 1129–34.
72. D. Srolovitz, M.J. Luton, R. Petkovic-Luton, D.M. Barnett, and W.D. Nix: *Acta Metall.*, 1984, vol. 32, pp. 1079–88.
73. E. Arzt and D. Wilkinson: *Acta Metall.*, 1986, vol. 34, pp. 1893–98.
74. J. Rosler and E. Arzt: *Acta Metall. Mater.*, 1988, vol. 36, pp. 1043–51.
75. F.W. Crossman and M.F. Ashby: *Acta Metall.*, 1975, vol. 23, pp. 425–40.